

Journal Name

COMMUNICATION

Exploiting Kinetics for Assembly of Multicomponent Nanoparticle Networks with Programmable Control of Heterogeneity

Received Accepted

Jessica L. Davis, a Karunamuni L. Silva, a and Stephanie L. Brock

DOI: 10.1039/x0xx00000x

www.rsc.org/

Kinetic control of metal chalcogenide nanoparticle oxidative assembly is realized by varying the redox potential of the chalcogenide, structure (wurtzite vs. zinc blende), and ligand chain length. This knowledge is exploited to form two-component (ZnS + CdSe) hybrid aerogels with minimal heterobonding (phase-segregated) or maximal heterobonding (intimately mixed).

In order to address current challenges in sustainable energy production and storage, complex materials comprising multiple components working in harmony (or, better yet, synergy) to achieve processes including energy transformation (photovoltaics, thermoelectrics, photocatalysis) and charge transport and storage (batteries), are needed (1). Nanoparticles are an important part of the clean energy revolution because their size produces a large surface area with which to interact with the environment (catalytic transformations, sensing), with properties (optical, magnetic, electronic) that can be tuned by size or chemical modification (2-5). Solution-phase routes are often embraced for the synthesis of discrete nanoparticles because they enable exquisite control over size, shape and surface functionality, and hence the native properties (6). However, applications requiring collection or dispersion of charge (i.e., transport properties) require nanoparticles to be physically "wired" into a connected network, necessitating the formation of interparticle bonds that are robust and enable charge transport (1, 7-9). Unfortunately, the success of solution phase routes rests to a large extent on the use of long-chain organic capping groups that regulate the synthesis (allowing size and shape targeting) and stabilize the resultant particles against aggregation (10, 11). These organic ligands are electrically

The Brock group has developed a methodology for assembly of

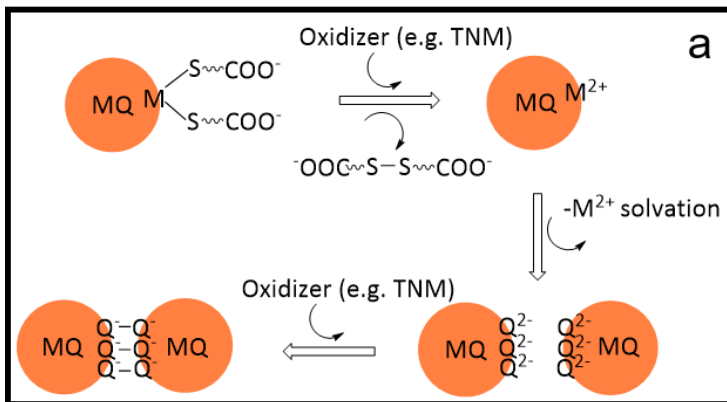
metal chalcogenide nanoparticles into gels and films predicated on solution-phase oxidative removal of surface thiolates, followed by oxidative crosslinking of the (subsequently exposed) surface chalcogenides via chalcogenide bonds (Fig. 1a). This oxidative assembly approach is general and has been exploited for the assembly of MQ (M = Cd, Pb; Q = S, Se, Te), ZnS and Bi₂Te₃ nanoparticles into singlecomponent porous architectures (gels and aerogels) (20-30). Two component systems have also been realized by starting with core@shell nanoparticles, specifically CdSe@ZnS, producing both aerogels and thin films (22, 27, 28). While other groups have shown that metal chalcogenide components can be assembled with metal nanoparticles to make composite aerogels, CdTe-Au (31, 32) and CdSe-Ag (33), to our knowledge, there are no examples of multicomponent chalcogenide gels comprising two distinct nanoparticle components, (e.g., CdSe-ZnS). This "materials gap" arises in part due to the difficulty in controlling phase segregation due to differences in the reaction rates of the two components (14), a problem well-established in co-precipitation syntheses.

insulating, precluding the desired solid-state charge transport, and generally reducing physical contact with the environment (12). Methods enabling rational integration of colloidal nanoparticles into functional architectures that are capable of maintaining the high surface area intrinsic to discrete nanoparticles, via chemical linkages that facilitate interparticle charge transport, and enable controlled placement of multiple complementary components, are lacking (13-15). The ability to program the assembly of distinct nanocrystals into 2- and 3-D electronically conductive networks with control over phase segregation would permit coupling of orthogonal properties within a single material, in an arrangement that enables the complex functionality needed to achieve more efficient solar cells (p + n-type semiconductor, bulk nanoheterojunction architecture (16-18))or photosensitized catalysts (semiconductor + catalyst, homogeneous mixture (3, 19)).

^{a.} Department of Chemistry, Wayne State University, Detroit, MI 48202 USA Email: sbrock@chem.wayne.edu.

[†]Electronic Supplementary Information (ESI) available: Synthesis and characterization procedures for metal chalcogenide nanocrystals (NCs) and aerogels and corresponding PXRD and TEM data; TR-DLS of the oxidative assembly of CdS NCs as a function of ligand chain-length; size histograms for NCs; images of single component gels; TEM image of co-gels with lattice fringes; zeta potential plots of NCs; raw ICP-MS data and TEM-EDAX data for co-gels. See DOI: 10.1039/x0xx00000x

COMMUNICATION Journal Name



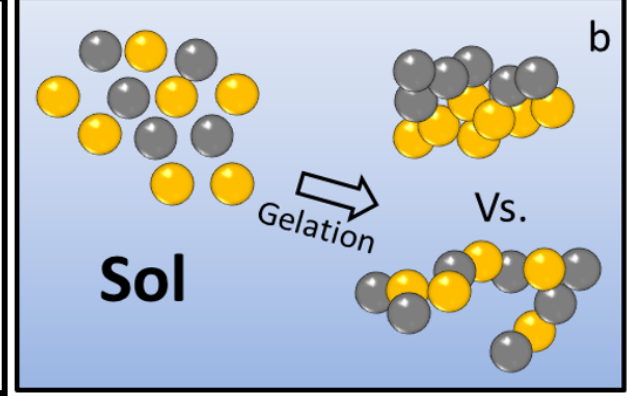


Figure 1. a) Scheme for sol-gel synthesis of metal chalcogenide assemblies involving (1) irreversible ligand loss by oxidation of thiolates to disulfides (TNM = tetranitromethane; (2) solvation of surface metal ions to reveal underlying chalcogenide; and (3), oxidation of surface chalcogenides to form dichalcogenide crosslinkers that knit the gel together. b) Types of hetero- or homogeneous systems that can be produced through tuning the kinetics of colloidal aggregation; intimate mixing (bottom) is desirable for photosensitized catalysts to enable facile transport of charges and energy between the two components throughout the specimen whereas phase-segregation (top) is beneficial for bulk nanoheterojunction solar cells where transport between the two components occurs only at the interface so that photogenerated carriers can be extracted.

Work in our group has shown that the kinetics of aggregation of II-VI type colloidal NCs is directly affected by the oxidant concentration, NC concentration, NC size, crystal structure, and the ease of oxidation of the chalcogenide (Q) (22, 30). Notably, the redox properties of Q strongly impact the kinetics, with tellurides gelling rapidly relative to selenides, themselves more rapid than sulfides, all other factors being equal (26). Thus, in practice, co-gelation of tellurides and sulfides would be expected to lead to minimal mixing. This can be mitigated (or exacerbated) by the effect of the native structure (zinc blende, zb vs. wurtzite, w) as zb exhibits slow kinetics relative to w. In the present work we show that the kinetics can also be tuned independently by altering the capping ligand, and that judicious use of these tools allows us to tailor the kinetics of aggregation in solution to favor heterobonding between dissimilar particles, leading to well-mixed composites; or favor homobonding, leading to phase-segregation (Figure 1b).

From examination of Figure 1a, it is evident that the first step in the oxidative assembly process is the oxidation of surface thiolates, which must proceed by penetration of the oxidant

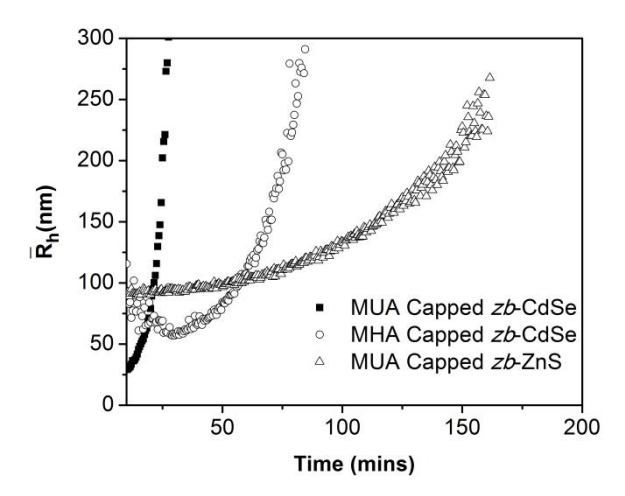


Figure 2. Time evolution as a function of hydrodynamic radius (\mathbf{R}_h) vs. metal and capping ligands, for zb-MQ NC CdS sols of concentration 3 x 10^{-7} M (3 ml sol) to which 20 μ l of 3% aq. TNM (oxidant) is added.

through the hydrocarbon tail of the capping ligand to the thiolate head-group. Accordingly, we predicted that deprotection of longer chain thiolates would proceed by slower kinetics than shorter chain thiolates. This premise is validated by a time-resolved dynamic light scattering (TR-DLS) study of 4.3 ± 0.4 nm wurtzite-CdS nanocrystals using 16-mercaptohexadecanoic acid (MHA, C16 hydrocarbon chain) vs. 11-mercaptoundecanoic acid (MUA, C11 hydrocarbon chain) as capping ligands (Figures S1, S2). Based on the evolution of the hydrodynamic radius as a function of time, MHA-capped CdS oxidative assembly proceeds at a much slower rate than when MUA is used as the capping agent, requiring twice as long (10 min) to achieve a radius of ca. 150 nm.

As a test case for controlled heterogeneity in multicomponent systems, we elected to use CdSe and ZnS nanocrystals because they together comprise 4 different elements, thereby enabling us to distinguish between aggregative assembly processes and possible ion-exchange processes using chemical mapping and physical property characterization. The thermodynamically stable structures for CdSe and ZnS nanocrystals are w and zb, respectively. Based on the redox properties of Q, we expect the kinetics of assembly of CdSe>>ZnS, and this difference will be made larger by the role of structure in kinetics (w>>zb). Accordingly, metastable zb-CdSe was employed in the study to better match the zb-ZnS (Figure S3, S4). Sizes for each were comparable (4.0 ± 0.6 nm for zb-ZnS; 4.2 ± 0.5 nm for zb-CdSe). zb-ZnS was capped exclusively with MUA whereas zb-CdSe was capped with either MUA or MHA.

TR-DLS studies show the relative rates of gelation to be MUA-CdSe>MHA-CdSe>MUA-ZnS based on the change in hydrodynamic radius as a function of time (Figure 2). As seen previously with the CdS NCs (Figure S2) the MHA-capped CdSe NCs had slower kinetics of aggregation than the MUA capped CdSe NCs; and both showed faster kinetics of aggregation relative to the *zb*-ZnS, due to the ease of oxidation of selenide relative to sulfide (34). Based on the kinetic data, we predict that mixtures of MUA-CdSe + MUA-ZnS will show a greater degree of phase-segregation (more homo-bonding between particles) than MHA-CdSe + MUA-ZnS (more heterobonding

Journal Name COMMUNICATION



Figure 3. a) The sol-gel transformation as a function of time for MUA-CdSe + MUA-ZnS treated with tetranitromethane (TNM). The yellow solution on top is the by-product of the oxidation by TNM, removed in the solvent exchange process. b) The sol-gel transformation for MHA-CdSe + MUA-ZnS treated with TNM. Representative images of single component gels are shown in Figure S5.

between particles), as shown in Figure 1b top and bottom, respectively.

For the co-gelation experiments, the concentration for each sample was prepared to be 4.8×10^{-6} M, and 1 ml each of CdSe and ZnS sols were combined in a glass vial. Following the combination of the two nanocrystalline sols, 20 µl of 3% TNM solution was added to the CdSe/ZnS sol and the sample was shaken. For the MUA-CdSe + MUA-ZnS combination, the large difference in oxidative assembly rates leads to rapid gelation of the CdSe component (<1 h), while the ZnS takes nearly a day to gel (Figure 3a). The result is a visibly phase-segregated gel with CdSe (orange) on the bottom and ZnS (white) on the top. By contrast, gelation of MHA-CdSe + MUA-ZnS occurs much slower, over 4-5 h, and no visible phase-segregation is evident (Figure 3b), which we attribute to slowing the kinetics of CdSe to better match ZnS, achieved by using a longer-chain thiolate on the former.

Following the gelation process the solvent was exchanged to remove the disulfide and oxidant by-products, and the samples were dried using supercritical CO₂ extraction. Despite the obvious phase-segregation, the samples are morphologically quite similar when imaged by TEM (Figure 4a, b), revealing the characteristic pearl-necklace morphology of colloidal aerogels. Likewise, PXRD data (Figure 4c) revealed virtually identical patterns for aerogels formed from MUA-CdSe + MUA ZnS and MHA-CdSe + MUA-ZnS, showing peaks for both zb-CdSe and zb-ZnS phases and no evidence of ion-exchanged phases (ZnSe, CdS) or alloys, suggesting the individual nanoparticle components remain intact within the structure. The diffusereflectance measurements are consistent with this analysis, with each gel showing two distinct absorption onsets at 2.3 eV and 3.6 eV, attributed to quantum-confined CdSe and ZnS, respectively (Figure 4d).

ICP-MS was employed on sonicated specimens of the aerogels and confirmed the overall 1:1 ratio of Cd:Zn in both of the cogels (Table S1). TEM-EDS data were acquired in multiple regions to better quantify the extent of phase segregation, collecting elemental analysis data on 200-300 nm areas of the grid. As shown in Table S2, quantification of Cd and Zn for the MUA-CdSe + MUA-ZnS co-gel indicates that the concentrations vary widely from spot-to-spot, and always have one element present in excess (typically large excess) over the other. In contrast, MHA-CdSe + MUA-ZnS co-gels often have a 1:1 ratio although in some spots one element is in excess. HR-TEM of the MHA-CdSe + MUA-ZnS co-gels also reveals the presence of both components on lengthscales of ~30 nm, as evidenced from their different lattice fringe spacing (Figure S6).

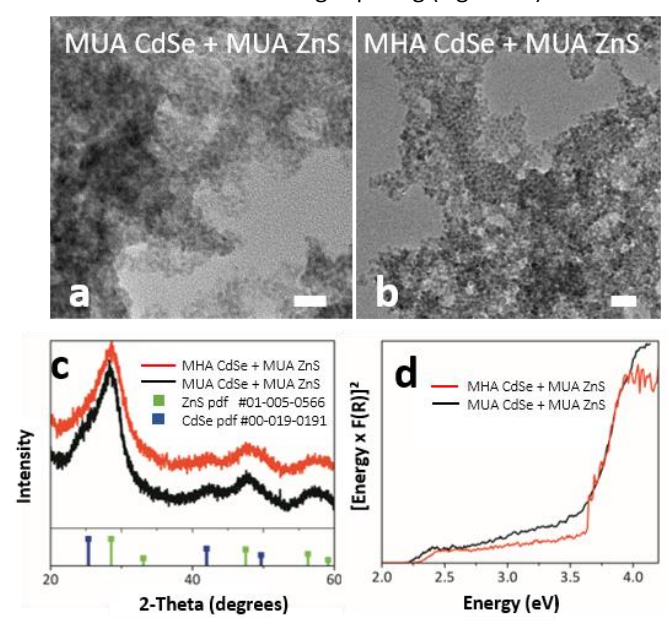


Figure 4. TEM micrographs (scale bar = 20 nm) of (a) the phase-segregated co-gel and (b) the intimately mixed co-gel. The corresponding PXRD diffraction patterns are shown in (c) and the Kubelka-Monk-approximated diffuse reflectance spectra are shown in (d).

To better assess mixing in the MHA-CdSe + MUA ZnS co-gels, element mapping was performed (Figure 5a). Clear evidence for localized phase segregation on the order of 10's to 100's of nm is apparent, attributed to the fact that while the kinetics of these two systems are more comparable than between MUA-CdSe + MUA-ZnS, the remaining difference precludes perfect mixing (Figure 2). Presumably, better kinetic matching (perhaps by the use of a shorter chain thiolate on ZnS) would enable more intimate mixing of the two components.

The kinetically-driven localized phase-segregation can be followed over the course of the gelation by zeta potential measurements of the net charge at the particle surface. Values for single component NC samples (MUA-ZnS, MUA-CdSe, MHA-CdSe), as well as a mixture of MUA-ZnS + MHA-CdSe, were around -50 mV, indicative of a stable colloidal solution of negatively charged NCs (Figure S7). However, when the oxidant is added to incite gelation in the MUA-ZnS + MHA-CdSe system, the zeta potential changes abruptly, approaching zero, and then adopting positive values, reflecting the weakening of the repulsive forces and the onset of aggregation

COMMUNICATION Journal Name

(Figure 5b). Rather than a smooth increase in zeta potential, two apparent onsets are evident. This likely reflects kinetic differences, with the CdSe assembling more quickly than ZnS

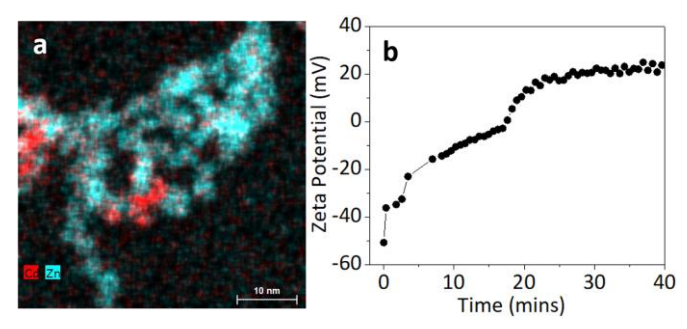


Figure 5. (a) STEM-EDS mapping of localized island formation of CdSe (red) in ZnS (teal) upon co-gelation of MHA-CdSe + MUA-ZnS; (b) Time dependence of zeta potentials of an MHA-CdSe + MUA-ZnS mixture after adding the oxidant (TNM).

An important concept in the design of heterogeneous composites is the ability to control the dispersion of nanocomponents and their interfaces to tune exchange pathways for carrier extraction or delivery, or create multiphase boundaries for selective catalysis. Here we show that the degree to which phase-segregation occurs in dualcomponent metal chalcogenide nanoparticle oxidative assembly can be rationally modified by understanding the kinetic contributors to single-component oxidative assembly. Importantly, fixed kinetic drivers such as redox properties of the chalcogenide or native structure of the nanocrystals can be compensated by changing the surface ligand that is oxidatively removed in the early stages of the assembly mechanism. While demonstrated for a single two-component system (CdSe + ZnS), the kinetic insights are expected to be transferrable to the wide range of metal chalcogenide NCs available and enable design of increasingly complex hybrids, enabling nanoscale functional control within macroscopic objects.

We acknowledge the NIH (R44 CA138013-03, via a subcontract from Weinberg Medical Physics, LLC) and the NSF (1709776, 0216084, 1427926) for funding, and thank FEI for providing STEM/EDS mapping data.

Conflicts of interest

There are no conflicts to declare.

Notes and references

- D. R. Rolison, J. W. Long, J. C. Lytle, A. E. Fischer, C. P. Rhodes, T. M. McEvoy, M. E. Bourg and A. M. Lubers, *Chem. Soc. Rev.*, 2009, 38, 226-252.
- X. Li, X. Hao, A. Abudula and G. Guan, J. Mater. Chem. A, 2016, 4, 11973-12000.
- N. Razgoniaeva, P. Moroz, S. Lambright and M. Zamkov, J. Phys. Chem. Lett., 2015, 6, 4352-4359.
- 4. C. R. Kagan, E. Lifshitz, E. H. Sargent and D. V. Talapin, *Science*, 2016, **353**.
- G. H. Carey, A. L. Abdelhady, Z. Ning, S. M. Thon, O. M. Bakr and E. H. Sargent, *Chem. Rev.*, 2015, 115, 12732-12763.

- 6. J. Chang and E. R. Waclawik, RSC Adv., 2014, 4, 23505-23527.
- J. J. Pietron, R. M. Stroud and D. R. Rolison, *Nano Lett.*, 2002, 2, 545-549.
- 8. D. R. Rolison, Science 2003, 299, 1698-1701.
- 9. C. Ziegler, A. Wolf, W. Liu, A.-K. Herrmann, N. Gaponik and A. Eychmüller, *Angew. Chem. Int. Ed.*, 2017, **56**, 13200-13221.
- Y. Yang, H. Qin, M. Jiang, L. Lin, T. Fu, X. Dai, Z. Zhang, Y. Niu, H. Cao, Y. Jin, F. Zhao and X. Peng, *Nano Letters*, 2016, 16, 2133-2138.
- 11. Y. Yang, H. Qin and X. Peng, Nano Lett., 2016, 16, 2127-2132.
- 12. J.-Y. Kim and N. A. Kotov, Chem. Mater., 2014, 26, 134-152.
- F. Lübkemann, J. F. Miethe, F. Steinbach, P. Rusch, A. Schlosser,
 D. Zámbó, T. Heinemeyer, D. Natke, D. Zok, D. Dorfs and N. C. Bigall, Small, 2019, 15, 1902186:1902181-1902188.
- B. Cai, V. Sayevich, N. Gaponik and A. Eychmüller, *Adv. Mater.*, 2018, 30, 1707518.
- D. Wen and A. Eychmüller, Chem. Comm., 2017, 53, 12608-12621.
- A. K. Rath, M. Bernechea, L. Martinez, F. P. G. de Arquer, J. Osmond and G. Konstantatos, Nat Photon, 2012, 6, 529-534.
- A. K. Rath, F. Pelayo Garcia de Arquer, A. Stavrinadis, T. Lasanta, M. Bernechea, S. L. Diedenhofen and G. Konstantatos, Adv. Mater., 2014, 26, 4741-4747.
- 18. Y. Xie, Q. Tan, Z. Zhang, K. Lu, M. Li, W. Xu, D. Qin, Y. Zhang, L. Hou and H. Wu, *J. Mater. Chem. C*, 2016, **4**, 6483-6491.
- T. O'Connor, M. S. Panov, A. Mereshchenko, A. N. Tarnovsky, R. Lorek, D. Perera, G. Diederich, S. Lambright, P. Moroz and M. Zamkov, ACS Nano, 2012, 6, 8156-8165.
- J. L. Mohanan, I. U. Arachchige and S. L. Brock, *Science*, 2005, 307, 397-400.
- I. U. Arachchige and S. L. Brock, Acc. Chem. Res, 2007, 40, 801-809.
- I. U. Arachchige and S. L. Brock, J. Am. Chem. Soc., 2007, 129, 1840-1841.
- 23. I. R. Pala, I. U. Arachchige, D. G. Georgiev and S. L. Brock, *Angew. Chem. Int. Ed.*, 2010, **49**, 3661-3665.
- S. Ganguly and S. L. Brock, J. Mater. Chem., 2011, 21, 8800-8806.
- 25. Q. Yao and S. L. Brock, Inorg. Chem., 2011, 50, 9985-9992.
- L. Korala and S. L. Brock, J. Phys. Chem. C, 2012, 116, 17110-17117.
- 27. L. Korala, L. Li and S. L. Brock, *Chem. Comm.*, 2012, **48**, 8523-8525.
- L. Korala, Z. Wang, Y. Liu, S. Maldonado and S. L. Brock, ACS Nano, 2013, 7, 1215-1223.
- N. Gaponik, A. Wolf, R. Marx, V. Lesnyak, K. Schilling and A. Eychmüller, Adv. Mater., 2008, 20, 4257-4262.
- 30. S. Ganguly, C. Zhou, D. Morelli, J. Sakamoto and S. L. Brock, *J. Phys. Chem. C*, 2012, **116**, 17431-17439.
- T. Hendel, V. Lesnyak, L. Kühn, A.-K. Herrmann, N. C. Bigall, L. Borchardt, S. Kaskel, N. Gaponik and A. Eychmüller, *Adv. Funct. Mater.*, 2013, 23, 1903-1911.
- 32. V. Lesnyak, A. Wolf, A. Dubavik, L. Borchardt, S. V. Voitekhovich, N. Gaponik, S. Kaskel and A. Eychmüller, *J. Am. Chem. Soc.*, 2011, **133**, 13413-13420.
- L. Nahar, R. J. A. Esteves, S. Hafiz, Ü. Özgür and I. U. Arachchige, ACS Nano, 2015, 9, 9810-9821.
- 34. M. Bouroushian, *Electrochemistry of Metal Chalcogenides*, Springer Berlin Heidelberg, 2010.